Journal of Power Sources 209 (2012) 257–261

Contents lists available at SciVerse ScienceDirect

Journal of Power Sources

journal homepage: www.elsevier.com/locate/jpowsour

Short communication

Effect of annealed treatment on microstructure and cyclic stability for La–Mg–Ni hydrogen storage alloys

J. Gao [a], X.L. Yan [b], Z.Y. Zhao [b], Y.J. Chai [b,*], D.L. Hou [a]

[a] School of Physics Science and Information Engineering, Hebei Normal University, Hebei, Shijiazhuang 050024, China
[b] School of Chemistry and Materials Science, Hebei Normal University, Hebei, Shijiazhuang 050024, China

ARTICLE INFO

Article history:
Received 17 October 2011
Received in revised form 3 February 2012
Accepted 22 February 2012
Available online 2 March 2012

Keywords:
Hydrogen storage materials
Cyclic stability
Metal hydride
Annealed treatment

ABSTRACT

The influence of annealed treatment on the microstructure and the cyclic stability for La–Mg–Ni alloys are systematically investigated by FESEM-EDX, XRD, PCT and electrochemical measurements. It is demonstrated that Ni and La are almost evenly dispersed, but Mg is nonuniform distribution in these alloys. Rietveld analysis results illustrate that the alloys mainly consist of $LaNi_5$, Pr_5Co_{19}-type, Ce_2Ni_7-type and $PuNi_3$-type phases. The mass fraction of each phase in these alloys varies after annealed. The 3d annealed alloy shows the better hydriding/dehydridng capacity and electrochemical cyclic stability. As annealed time is continually prolonged, the hydrogen storage capacity slightly increases, but the electrochemical discharge capacity decreases. Estimating from the pressure-composition isotheral curves, it is considered that the hydriding of these alloys is governed by two processes: the initial process can be expressed by the hydriding of the phases with stacking of $[LaMgNi_4]$ and $[LaNi_5]$ slabs and the second is controlled by $LaNi_5$ phase.

1. Introduction

La–Mg–Ni series alloys are extensively investigated in the past decade due to their high hydrogen storage capacity and good electrochemical properties compared to AB_5-type alloys. However, to date, the poor cyclic stability hinders its application as negative electrode materials of Ni-MH batteries or hydrogen storage media. To meliorate this problem, a series of studies including metal substitution [1–4], mechanical milling [5,6] and various preparation techniques [7–9] have been reported. In addition, making the alloys homogenous by annealed treatment also is an important method to improve hydrogen storage properties of La–Mg–Ni alloys [10].

General, La–Mg–Ni alloys mainly consist of $PuNi_3$-type, Ce_2Ni_7-type or Pr_5Co_{19}-type phase [11]. The crystal structure of these phases is a stacking of $[LaMgNi_4]$ (Laves-type) and $[LaNi_5]$ ($CaCu_5$-type) slabs along [0 0 1] axis. Moreover, the stacking structure of these phases has polymorphism with either a hexagonal (2H) or a rhombohedral (3R) structure [12]. The composition and the hydrogen storage properties are affected by the annealed treatment and the cooled procedure. Different opinions between composition and the improved hydrogen storage properties for annealed La–Mg–Ni alloys are presented. Huang et al. [13] reported that $La_{0.98}Ni_{5.03}$ phase appeared in annealed $La_{0.78}Mg_{0.22}Ni_{3.48}Co_{0.22}Cu_{0.12}$ alloys. And the decrease of the lattice parameter of $La_{0.98}Ni_{5.03}$ resulted in the increase of the reversible hydrogen capacity. Guo et al. [14] found $La_{2-x}Ti_xMgNi_9$ consisted of $LaNi_5$, $LaMg_2Ni_9$ (3R) and $LaNi_3$. Annealing $La_{2-x}Ti_xMgNi_9$ at 800–900 °C lowered the capacity degradation and prolonged the cycling lifetime because of the improvement of the compositional homogeneity. Quenching La–Mg–Ni alloys from 840 °C resulted in the formation of $(La,Mg)_2Ni_7$, La_4MgNi_{19} (2H and 3R) and $LaNi_5$ phase [15]. Rapidly quenching $La_2Mg(Ni_{0.85}Co_{0.15})_9$ alloy composed of $PuNi_3$-type phase and $LaNi_5$ phase enhanced the electrochemical cyclic stability due to the grain refinement and the formation of an amorphous phase [16]. In the present work, the alloys are composed of multiple phases. The cyclic stability and the equilibrium hydrogen pressure for these alloys adjust to the change of mass fraction. Therefore, the goal of this work focuses on the relationship between the microstructure, composition and the hydriding/dehydriding and electrochemical cyclic stability for annealed La–Mg–Ni alloys.

2. Experimental

La and Ni were firstly melted by induction melting under the atmosphere of argon. Then Mg was poured into the melting alloy. To compensate for the volatility losses of Mg, excess Mg was added. Finally, the as-cast bulk alloys were placed in quartz tube and annealed at 800–900 °C for 3d and 5d under a flow of argon.

* Corresponding author. Tel.: +86 311 86269377; fax: +86 311 86269377.
E-mail address: yjchaiwn@gmail.com (Y.J. Chai).

0378-7753/$ – see front matter © 2012 Elsevier B.V. All rights reserved.
doi:10.1016/j.jpowsour.2012.02.088

The microstructure analysis and chemical composition of La–Mg–Ni were investigated by means of an S-4800 field-emission scanning electron microscope (FE-SEM) and Energy dispersive X-ray spectroscopy (EDX). XRD measurement was carried out on X'pert PRO MPD X-ray diffractometer with Cu Kα radiation in the range from 10° to 90° with 0.02° min^{-1}.

Before the measurement of pressure-composition isothermal (PCI) curves by Sievert's apparatus, the sample was evacuated at 200 °C and 1×10^{-4} Pa for at least 2 h in resistance furnace to remove the impurities. Then, the alloys were hydrided under a hydrogen pressure of ~5 MPa and dehydrided to ~0.001 MPa to measure the hydriding/dehydridng cyclic stability. After 30 cycles, the PCI curves were measured at 40 °C, 70 °C and 100 °C.

The alloy and porous nickel powder were mixed in a weight ratio of 1:5 and cold pressed the mixture to form $\Phi = 1$ cm pellets. Subsequently, the simulated three-electrode cell including a working electrode (metal hydride electrode), a counter electrode ($NiOOH/Ni(OH)_2$) and a reference electrode (Hg/HgO) was installed. Prior to electrochemical testing, all alloy electrodes were immersed in 6 M KOH aqueous solution for 2d to wet them fully. Finally, the cell was first charged/discharged at current density of 60 mA g^{-1} to reach the maximum capacity. Then they were charged at 120 mA g^{-1} for 4 h and discharged at 120 mA g^{-1} to the cut-off voltage −0.6 V.

3. Results and discussion

3.1. Microstructure

The typical SEM-EDX analysis and chemical composition of La–Mg–Ni alloys are shown in Fig. 1 and Table 1. It can be seen that Ni and La elements are evenly scattered in two domains. Moreover, the atomic ratio of La and Ni in A domain is close to 1:5, which suggests La and Ni prefers to form $LaNi_5$ compound prepared by this approach. Mg is detected to show the nonuniform distribution in A and B domains for all the samples. Namely, the apparent atomic ratio of La, Mg and Ni in B is close to 4:1:19 (La_4MgNi_{19}) or 3:1:14 (La_3MgNi_{14}). But it cannot determine the definite composition of each phase by SEM or EDX results due to the closed composition. In addition, the elemental analysis of La, Mg and Ni in the whole domain coincides with ICP chemical analysis [17]. It is found to be near $La_{0.81}Mg_{0.19}Ni_{3.9}$, which complies with the nominal composition.

Based on the aforementioned results, XRD data of these alloys were mainly refined using a four phase model including Pr_5Co_{19}-type (La_4MgNi_{19}, 2H), Ce_2Ni_7-type (La_3MgNi_{14}, 2H), $PuNi_3$-type (La_2MgNi_9, 3R) and $LaNi_5$. The refinement results are shown in Fig. 2 and Table 2. The mass fraction of $LaNi_5$, Pr_5Co_{19}-type, Ce_5Co_{19}-type and $PuNi_3$-type phase is ~60%, ~21%, ~7% and ~12%, respectively, for as-cast La–Mg–Ni alloy. It varies after annealed treatment due to the short-range atomic migration [15]. The mass fraction of $LaNi_5$ decreases to 52% (annealed 3d) and 48% (annealed 5d). It also reduces for $PuNi_3$-type. Contrary, it enhances from 21% to 32% for Pr_5Co_{19}-type and from 7% to 16% for Ce_2Ni_7-type.

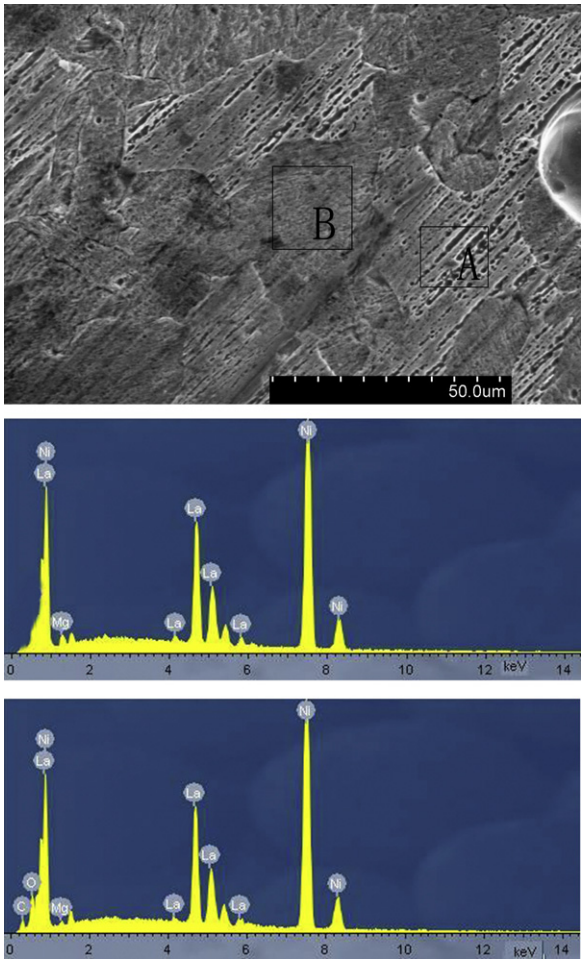

Fig. 1. Typical SEM-EDX analysis of La–Mg–Ni alloys.

3.2. Hydriding/dehydriding and electrochemical cyclic stability

Fig. 3 shows the hydriding/dehydriding cycles of La–Mg–Ni alloys at 70 °C. Two plateaus are observed in the initial cycles for all the alloys. It presents two hydriding processes judging from the plateau pressure. The equilibrium pressure of $PuNi_3$-type, Pr_5Co_{19}-type or Ce_2Ni_7-type phase is close to each other duo to their similar stacking structure. It is ~0.2 MPa after the partial substitution of La by Mg and ~0.7 MPa for $LaNi_5$. Therefore, it is regarded that the initial hydriding process is controlled by those phases and then by $LaNi_5$.

As for as-cast alloy, only one plateau with the width of 0.85 wt% is left after 30 cycles. Corresponding, an obvious decrease of hydrogen storage capacity from 1.44 wt% to 1.22 wt% is observed. $PuNi_3$-type phase is relatively easy to be amorphous in hydriding/dehydriding cycles because of the lattice strain in [La_2Ni_4] slab [18]. The mass fraction of $PuNi_3$-type phase is 12% in as-cast alloy. Moreover, Pr_5Co_{19}-type and Ce_2Ni_7-type phases occupy 28%. In view of the variation of PCI curves, it is presumed that these

Table 1
Element compositions of the phases for La–Mg–Ni alloys.

	Mapping	La (wt%)	Mg(wt%)	Ni (wt%)	La:Mg:Ni (atomic ratio)
As-cast alloy	A	32.5	0.6	66.9	1:0:4.9
	B	33.22	1.48	65.3	3.81:18
Annealed 3d	A	34.04	0.52	65.44	1:0:4.6
	B	33.42	1.94	64.64	3:1:13
Annealed 5d	A	33.76	0.73	65.5	1:0:4.6
	B	34.03	2.18	63.79	3:1:12

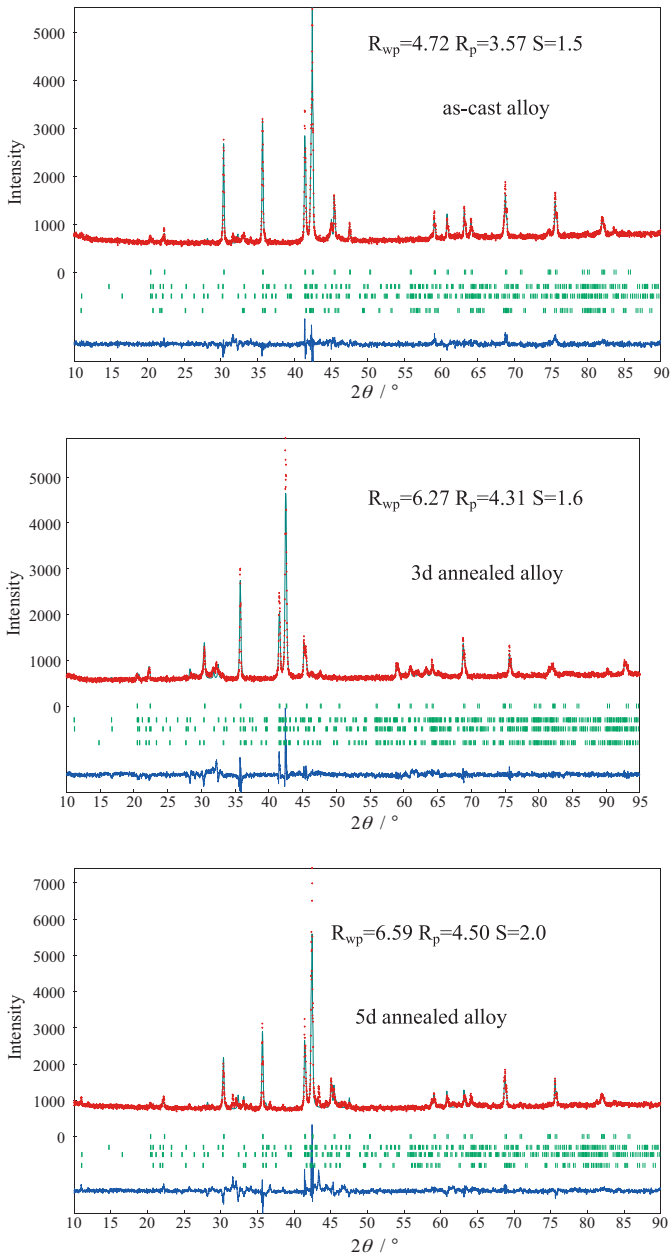

Fig. 2. Rietveld refinement of XRD patterns for La–Mg–Ni alloys. $LaNi_5$, Pr_5Co_{19}-type (2H), Ce_2Ni_7-type (2H) and $PuNi_3$-type (3R) are used as the model. The difference between the observed and calculated profiles is shown below the vertical bars.

phases in as-cast alloy tend to form the amorphous phase in hydriding/dehydriding process.

An obvious difference in PCI curves between as-cast alloy and annealed alloy is observed. It is two plateaus remains even after 30 hydriding/dehydridng cycles. Meanwhile, the plateau width with a pressure of 0.6–0.8 MPa shortens to 0.63 wt% and 0.48 wt%, respectively, and other extends. This indicates that the decreased content for $LaNi_5$ and the increased for Mg-contained phases after annealed. It coincides with the variation of mass fraction for all the phases in the alloys. The crystal structure of Ce_2Ni_7-type and Pr_5Co_{19}-type phases is a alternative combination of [$LaMgNi_4$] slab and n[$LaNi_5$] (n = 2, 3) slabs along c axis [19]. Hydrogen randomly occupies the interstitial site in [$LaMgNi_4$] and [$LaNi_5$] slabs in hydriding [15,20]. Therefore, the hydrogen storage capacity is slightly increased due to the increased mass fraction. It is 1.50 wt% for annealed 3d and 1.58 wt% for annealed 5d. The even occupation in [$LaMgNi_4$] and [$LaNi_5$] slabs results in the isotropic expansion, which reduces the lattice strain and postpones the amorphous. Consequently, the remnant hydrogen storage capacity after 30 cycles retains ~1.40 wt%.

In order to further illustrate the influence of phases, the hydriding/dehydriding curves for annealed alloys after 30 cycles were measured at different temperature, as shown in Fig. 4. Although no apparent change in the total hydrogen capacity for 3d annealed alloy is observed, the plateau width slightly is prolonged with increasing temperature. And the capacity is evidently increased for 5d annealed alloy. It is reported that a decreased capacity was observed for $LaNi_5$ alloy from 21 °C to 81 °C [21]. Otherwise, partial stable hydride is remained in lattice in hydriding/dehydriding for La–Mg–Ni alloys [22]. Hydrogen is released with increasing temperature. Therefore, the increased capacity is conjectured to be related to Mg-contained Pr_5Co_{19}-type or Ce_2Ni_7-type phases.

Fig. 5 shows the electrochemical cyclic stability of La–Mg–Ni alloys with charging/discharging at the current density of 120 mA g^{-1}. The discharge capacity of as-cast alloy rapidly decreases from 360 mAh g^{-1} to 220 mAh g^{-1} (100 cycles). It may be caused by the formation of amorphous phase in charging/discharging. The electrochemical cyclic stability of Mg-contained alloys was improved owing to the control of phase abundance for Pr_5Co_{19}-type (2H, 3R) or Ce_2Ni_7-type phase (2H) [23–25]. In addition, $LaNi_5$-type phase acts as the electrocatalyst to accelerate the electrochemical reaction in Mg-contained alloys, as proposed by Pan et al. [26]. In this case, the mass fraction of $LaNi_5$ phase decreases after annealed, which means the decrease of electrochemical reaction velocity. The increased mass fraction and their preservation in charging/discharging process for Pr_5Co_{19}-type and Ce_2Ni_7-type phases support the cyclic stability. The cooperation of two factors makes the discharge capacity keep 310–320 mAh g^{-1} and remain 270 mAh g^{-1} after 100 cycles for 3d annealed alloy. The mass fraction of $LaNi_5$ phase reduces with increasing annealed time, which leads to the capacity (296 mAh g^{-1}) slightly decreasing.

Table 2
Lattice parameters and mass fraction of La–Mg–Ni alloys.

		a (Å)	c (Å)	V (Å^3)	Phase abundance (%)
As-cast	$CaCu_5$-type	5.0311	3.990	87.47	60
	Pr_5Co_{19}-type	5.0336	32.28	708.3	21
	Ce_2Ni_7-type	5.0325	24.13	529.2	7
	$PuNi_3$-type	5.0343	24.36	534.6	12
Annealed 3d	$CaCu_5$-type	5.0311	3.989	87.45	52
	Pr_5Co_{19}-type	5.0294	32.22	705.7	25
	Ce_2Ni_7-type	5.0341	24.11	529.2	16
	$PuNi_3$-type	5.0344	24.36	534.7	7
Annealed 5d	$CaCu_5$-type	5.0327	3.992	87.57	48
	Pr_5Co_{19}-type	5.0348	32.21	707.3	32
	Ce_2Ni_7-type	5.0324	24.13	529.2	11
	$PuNi_3$-type	5.0294	24.23	530.8	9

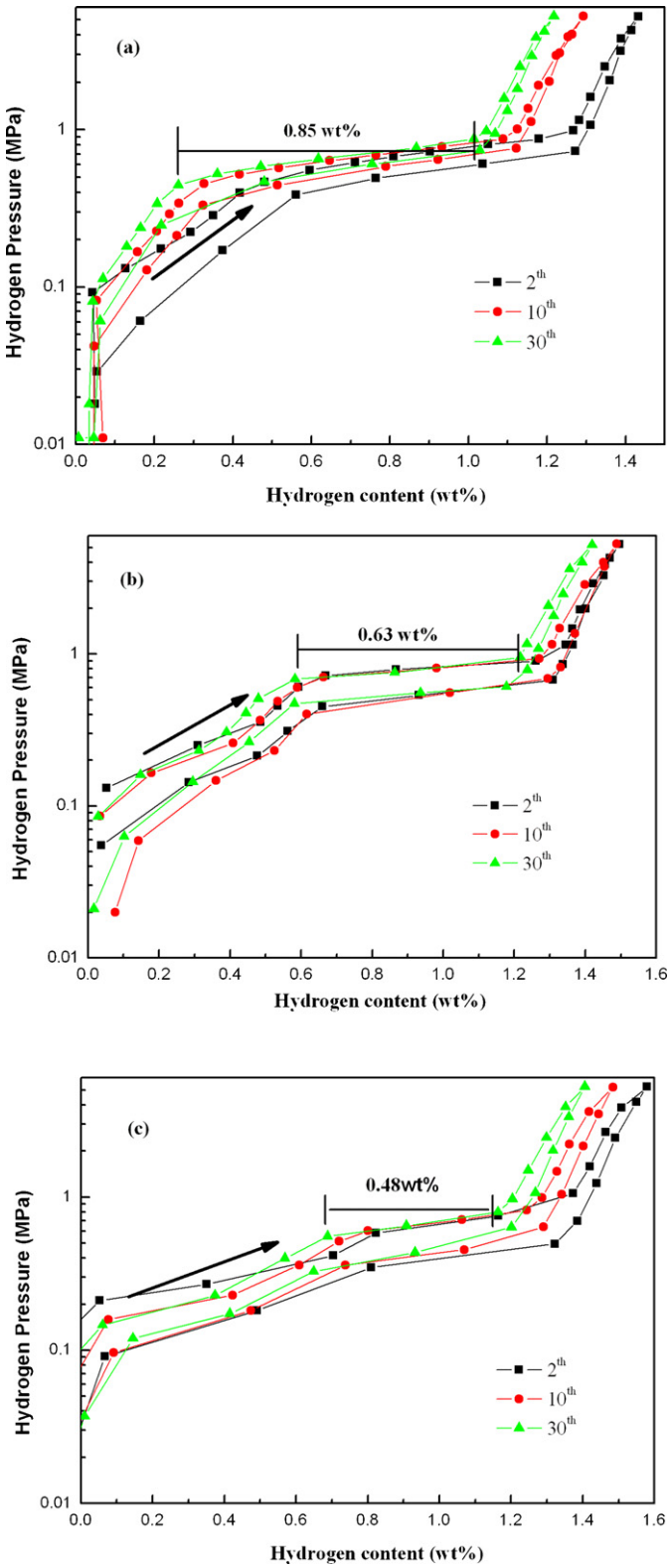

Fig. 3. Hydriding/dehydriding cycles of La–Mg–Ni alloys at 70 °C (a) as-cast alloy, (b) 3d annealed alloy, and (c) 5d annealed alloy.

These results suggest that the coexistence both Ce_2Ni_7-type and Pr_5Co_{19}-type phases with good stability and the electrocatalyst phase ($LaNi_5$) are important for the electrochemical cyclic stability of La–Mg–Ni series alloys.

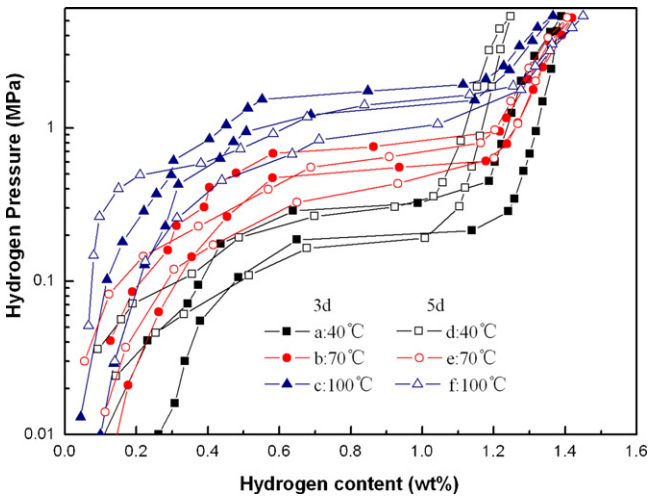

Fig. 4. PCI curves of annealed La–Mg–Ni alloys at 40 °C, 70 °C and 100 °C (a–c) 3d annealed alloy (d–f) 5d annealed alloy.

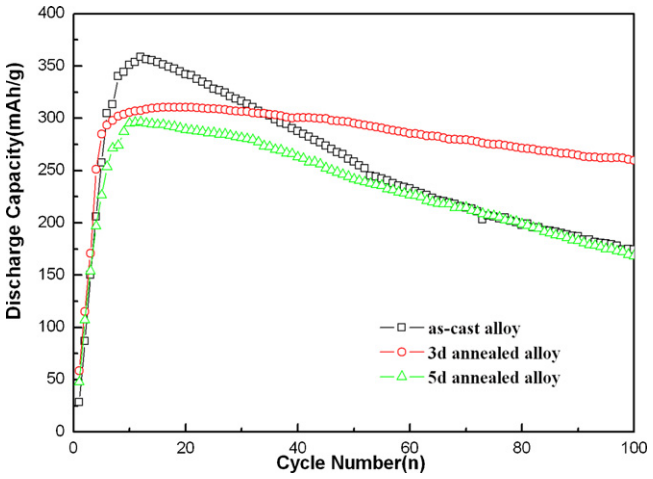

Fig. 5. Electrochemical cyclic stability of La–Mg–Ni alloys with charging/discharging at the current density of 120 mA g^{-1}.

4. Conclusions

The relationship between the microstructure, composition and the cyclic stability for La–Mg–Ni alloys are systematically investigated. FESEM-EDX results show that Ni and La are almost evenly scattered, but the composition of Mg-riched domain is close to La_3MgNi_{14} or La_4MgNi_{19}. Rietveld analysis results illustrate that it is mainly composed of $LaNi_5$-type, Pr_5Co_{19}-type, Ce_2Ni_7-type and $PuNi_3$-type phase. The mass fraction of $LaNi_5$ decreases from 60% to 48%, and it increases for other phases from 40% to 52%, respectively. Because of the difference of the equilibrium hydrogen pressure for these phases, two plateaus are observed in PCI curves. The hydrogen storage capacity after 30 cycles retains ~1.40 wt% and the discharge capacity remains 270 mAh g^{-1} after 100 cycles for 3d annealed alloy.

Acknowledgements

We acknowledge financial support from the National Natural Science Foundation of China (50901030) and Doctoral Science Foundation of Hebei Normal University (2007B12).

References

[1] Y.H. Zhang, X.P. Dong, S.H. Guo, G. Wang, J.Y. Ren, X.L. Wang, J. Alloys Compd. 398 (2005) 178–183.
[2] F. Zhang, Y. Luo, J. Chen, R. Yan, L. Kang, J. Chen, J. Power Sources 150 (2005) 247–254.
[3] W. Jiang, Z. Lan, W. Lou, L. Xin, J. Guo, Int. J. Hydrogen Energy 35 (2010) 11016–11024.
[4] T. Kohno, H. Yoshida, F. Kawashima, T. Inaba, I. Sakai, M. Yamamoto, M. Kanda, J. Alloys Compd. 311 (2000) L5–L7.
[5] M. Zhu, C.H. Peng, L.Z. Ouyang, Y.Q. Tong, J. Alloys Compd. 426 (2006) 316–321.
[6] D.J. Cuscueta, M. Melnichuk, H.A. Peretti, H.R. Salvaa, A.A. Ghilarducci, Int. J. Hydrogen Energy 33 (2008) 3566–3570.
[7] X. Dong, F. Liu, Y. Zhang, L. Yang, X. Wang, Mater. Chem. Phys. 108 (2008) 251–256.
[8] A. Férey, F. Cuevas, M. Latroche, B. Knosp, Bernard, Electrochim. Acta 54 (2009) 1710–1714.
[9] X. Zhang, D. Sun, W. Yin, Y. Chai, M.S. Zhao, J. Power Sources 154 (2006) 290–297.
[10] W. Hu, D. Kim, S. Jeon, J. Lee, J. Alloys Compd. 270 (1998) 255–264.
[11] H. Hayakawa, E. Akiba, M. Gotoh, T. Kohno, Mater. Trans. 46 (2005) 1393–1401.
[12] Y. Chen, C.A.C. Sequeira, X. Song, R. Neto, Q.D. Wang, Int. J. Hydrogen Energy 27 (2002) 63–68.
[13] T. Huang, J. Han, Y. Zhang, J. Yu, G. Sun, H. Ren, X. Yuan, J. Power Sources 196 (2011) 9585–9589.
[14] W.Q. Jiang, Z.Q. Lan, W.W. lou, J. Guo, Int. J. Hydrogen Energy 35 (2010) 11016–11024.
[15] Q.A. Zhang, M.H. Fang, T.Z. Si, F. Fang, D.L. Sun, L.Z. Ouyang, M. Zhu, J. Phys. Chem. C 114 (2010) 11686–11692.
[16] Y. Zhang, H. Ren, B. Li, X. Dong, Y. Cai, X. Wang, Mater. Charac. 58 (2007) 637–644.
[17] Z.Y. Liu, X.L. Yan, N. Wang, Y.J. Chai, D.L. Hou, Int. J. Hydrogen Energy 36 (2011) 4370–4374.
[18] R.V. Denys, A.B. Riabov, V.A. Yartys, M. Sato, R.G. Delaplane, J. Solid State Chem. 181 (2008) 812–821.
[19] Y. Khan, Acta Crystallogr. 30 (1974) 1533–1537.
[20] J. Nakamura, K. Iwase, H. Hayakawa, Y. Nakamura, E. Akiba, J. Phys. Chem. C 113 (2009) 5853–5859.
[21] H.H. Vanmal, K.H.I. Buschow, A.R. Miedema, J. Less-Common Met. 35 (1974) 65–76.
[22] Y.J. Chai, K. Sakaki, K. Asano, H. Enoki, E. Akiba, T. Kohno, Scripta Mater. 57 (2007) 545–548.
[23] S. Yasuoka, Y. Magari, T. Murata, T. Tanaka, J. Ishida, H. Nakamura, J. Power Sources 156 (2006) 662–666.
[24] T. Ozaki, M. Kanemoto, T. Kakeya, Y. Kitano, M. Kuzuhara, M. Watada, et al., J. Alloys Compd. 446–447 (2007) 620–624.
[25] H.G. Pan, Y.F. Liu, M.X. Gao, Y.F. Zhu, Y.Q. Lei, Q.D. Wang, Int. J. Hydrogen Energy 28 (2003) 113–117.
[26] Y.F. Liu, H.G. Pan, M.X. Gao, Y.Q. Lei, Q.D. Wang, J. Alloys Compd. 403 (2005) 296–304.